E-25-W16

REPORT DOCUMENTATION PAGE

Form Approved
OMB No. 0704-0188

1. AGENCY USE ONLY (Leave Blank)	2. REPORT DATE	3. REPORT TYPE AND DATES COVERED
	31 December 1995	1 June 1993 - 31 December 1995

4. TITLE AND SUBTITLE
The impact of scales and spatial distributions on small scale fluid loaded structural acoustic models

5. FUNDING NUMBERS
G N00014-93-1-0937

6. AUTHOR(S)
Kenneth A. Cunefare

7. PERFORMING ORGANIZATION NAME(S) AND ADDRESS(ES)

8. PERFORMING ORGANIZATION REPORT NUMBER

9. SPONSORING/MONITORING AGENCY NAME(S) AND ADDRESS(ES)
Office of Naval Research
Ballston Tower One
800 N. Quincy Street
Arlington, VA 22217-5660

10. SPONSORING/MONITORING AGENCY REPORT NUMBER

11. SUPPLEMENTARY NOTES COR:

12a. DISTRIBUTION/AVAILABILITY STATEMENT
Unlimited

12b. DISTRIBUTION CODE

13. ABSTRACT *(Maximum 200 words)*

The subject research addressed the scale (dimension) at which an attached structure influences the response of another structure. Here, the attached structures, or features, represent internals of a larger, fluid-loaded structure. Inertial, elastic, and internally wave-bearing structures were considered. The research applied the surface variational principal (SVP) and Hamilton's principal to model the dynamics and acoustics of these coupled fluid-loaded systems. Paradigm structures were a plate in a baffle and a cylindrical shell. A basic function approach was used for representing surface velocities, acoustic pressures, and features. The resulting system of equations then indicated the degree of coupling between features of different scales, and of different scales within a structure. When compared against a point representation, different spatial distribution of the same features were shown to have greatest impact near fluid-loaded resonances. This indicates that greater modeling fidelity is required in such frequency regions. Away from resonances, feature representation had little impact on structural response.

14. SUBJECT TERMS
Structural acoustics, fluid loaded plate, surface variational principal, complexity

15. NUMBER OF PAGES
35

16. PRICE CODE

17. SECURITY CLASSIFICATION OF REPORT	18. SECURITY CLASSIFICATION OF THIS PAGE	19. SECURITY CLASSIFICATION OF ABSTRACT	20. LIMITATION OF ABSTRACT
Unclassified	Unclassified	Unclassified	Unlimited

FINAL REPORT TO ONR

Contract Number No: N00014-93-1-0937

R & T Project Number: 122tplf02-02

The Impact of Scales and Spatial Distributions on Small Scale Fluid Loaded Structural Acoustic Models

Principle Investigator: Kenneth A. Cunefare

School of Mechanical Engineering

Georgia Institute of Technology

ONR Final
(31 Dec 1995)

DISCLAIMER NOTICE

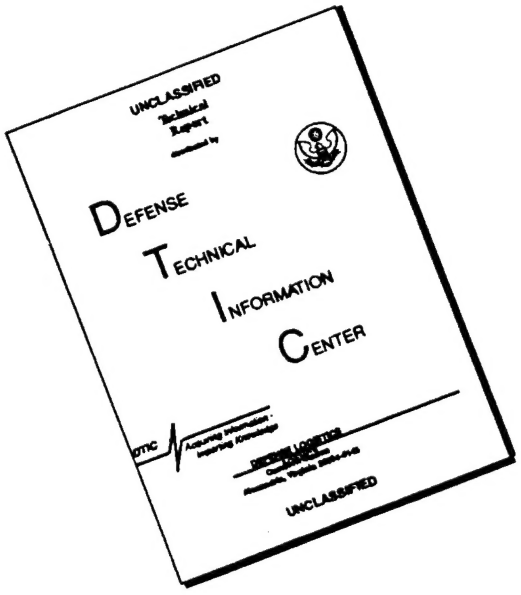

THIS DOCUMENT IS BEST QUALITY AVAILABLE. THE COPY FURNISHED TO DTIC CONTAINED A SIGNIFICANT NUMBER OF PAGES WHICH DO NOT REPRODUCE LEGIBLY.

I. SUMMARY OF RESEARCH

Most structural systems of naval relevance feature a variety of structural subsystems or subcomponents. These features often can have a drastic effect on the dynamic and acoustic behavior of a system, as evident in the vast amount of research. When predicting the dynamic and acoustic behavior of a system one must decide how much effort will be spent on modeling these smaller structural features. Consider, for example, a structural system that contains a simple mass element. The question arises, when does the size of this mass become large enough to justify a greater modeling effort? That is, can the mass be modeled using a lumped representation or must it be treated using some distributed representation? Moreover, how accurate must a spatial representation be to obtain a valid acoustic prediction? The same question can be posed for other structural subcomponents. The purpose of this work is to determine what, if any, system parameters influence the level of detail necessary to accurately represent the subcomponents of a structural-acoustic system. In conjunction with this research, the surface variational principle (SVP) was also extended for capped cylindrical shells.

To determine the impact of feature scales, a numerical interrogation of a simple fluid-loaded system was performed. This system consists of a semi-infinite plate that is simply supported in a rigid baffle which bounds the acoustic fluid. Inertial scale effects were investigated by considering an attached mass of varying dimension. Methods were also developed to study elastic scale effects through a spring-suspended mass and the scale effects of coupling two regions of the primary structure through a wave-bearing member supported by spring elements. Since closed form solutions to these types of problems are not readily available, the analysis was numerical in nature. The acoustic surface variational principle (SVP) is ideally suited to this research because it does not implement a surface discretization that has its own set of spatial scales. Note that the numerical techniques applied in this research, however, do not restrict the use of the results in other methods. The research focused on the influence the structural feature scales have on the structural-acoustic response of the entire system. The effect of feature scales on the radiated acoustic power under a general harmonic excitation, for example, was of particular interest.

Once the influence of these scales is identified, a greater understanding of how the size of a particular feature can affect the acoustic output of a system will be gained. Furthermore, future modeling efforts of structural-acoustic systems can be directed in a more efficient manner.

II. ANALYSIS METHOD

This section briefly outlines the variational method [1] as it applies to the semi-infinite plate [2] used for the numerical analyses discussed in the next section.

II.1 SVP for Plate System

The clean semi-infinite plate which is simply supported in a rigid baffle with one wetted surface is shown in Figure 1. Differential elements of surface area dA and dA' correspond to points $\mathbf{x}_S$ and $\mathbf{x}'_S$ on the surface of the plate or baffle. When the actual value of the surface pressure distribution, $\mathrm{Re}[p(\mathbf{x}_S)\exp(-i\omega t)]$, has been found, the variational quantity $\boldsymbol{J}$ will have a stationary value when an admissible virtual increment, $\delta p(\mathbf{x}_S)$, is applied. The variational principle states

$$\delta \boldsymbol{J} = 0$$

where $\boldsymbol{J}$ for a planar surface, fluid-loaded on one side, is given by

$$\begin{aligned} \boldsymbol{J} = 2\iint_{S'} \Big\{ & k^2 p(\mathbf{x}_S) p(\mathbf{x}'_S) - [\mathbf{n}(\mathbf{x}_S) \times \nabla p(\mathbf{x}_S)] \cdot [\mathbf{n}(\mathbf{x}'_S) \times \nabla' p(\mathbf{x}'_S)] \Big\} \\ & \times G(\mathbf{x}_S | \mathbf{x}'_S) dA' dA \; - \; i8\pi\omega\rho \int_S p(\mathbf{x}_S) v_n(\mathbf{x}_S) dA \end{aligned} \tag{1}$$

The variables are nondimensionalized as

$$\xi = \frac{x}{a}, \qquad p(x) = \rho c^2 \hat{p}(\xi), \qquad v_n = c\,\hat{v}_n(\xi). \tag{2}$$

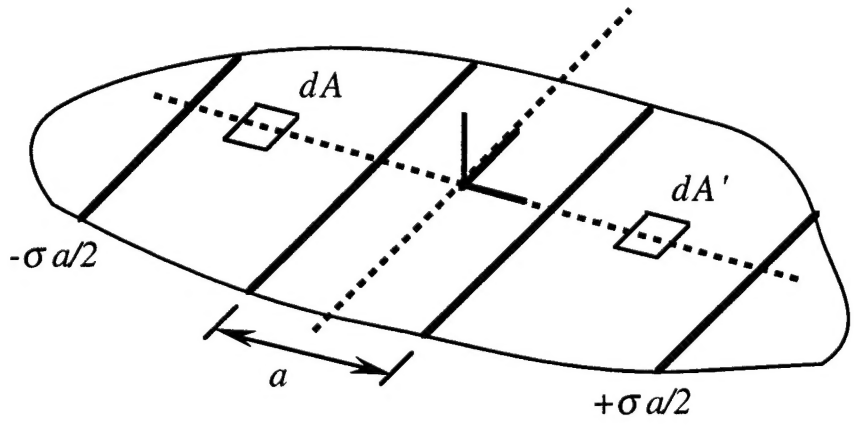

Figure 1. Semi-infinite fluid-loaded elastic plate in rigid baffle.

The nondimensionalized pressure and normal surface velocity are $\hat{p}$ and $\hat{v}_n$, respectively. The density, ρ, and sound speed, c, are for the acoustic fluid and a is the width of the plate. The carat can now be dropped since all the terms are nondimensional.

The surface pressure distribution is expressed using a Ritz expansion with N linearly independent basis functions as

$$p(\xi) = \sum_{i=1}^{N} \psi_i(\xi) P_i \tag{3}$$

where it is assumed the pressure vanishes beyond the distance $r=\sigma a/2$ [3, 4]. Therefore, it is only necessary that the functions, ψ, satisfy the condition

$$\psi_i(\xi) = 0, \quad \xi = \pm\frac{\sigma}{2} \tag{4}$$

and be both continuous and piece-wise differentiable. Similarly, the surface displacement is expressed as

$$w(\xi,t) = a\sum_{j=1}^{M} \phi_j(\xi) W_j(t), \quad -\frac{1}{2} \le \xi \le \frac{1}{2} \tag{5}$$

such that the basis functions, ϕ, are continuous, piece-wise differentiable, and satisfy the geometric boundary condition

$$\phi_j(\xi) = 0, \quad \xi = \pm\frac{1}{2}. \tag{6}$$

Note that M may be different from N. A harmonic time dependence is assumed for the generalized modal coordinate

$$q_j(t) = \mathrm{Re}[W_j \ \exp(-i\omega t)] \quad . \tag{7}$$

Therefore, the nondimensional normal surface velocity is

$$v_n(\xi,t) = -ika\sum_{j=1}^{M} \phi_j(\xi) W_j(t) \tag{8}$$

where $ka = a\omega/c$ is the nondimensional wavenumber and c is the wave speed in the acoustic fluid. By substituting these expansions into Eq.(2) and applying the variational principle,

$$\frac{\partial J}{\partial P_i} = 0, \quad i = 1,\ldots,N \tag{9}$$

a non-square system of equations is obtained relating the unknown modal pressure amplitudes, P_i, and unknown displacement amplitudes, W_j.

The remaining equations are the coupled equations for structural vibration. These are found by applying Lagrange's equation to the potential and kinetic energy expressions for the plate. The generalized forces are the force due to the harmonic excitation

$$Q_j^e = \rho c^2 a^2 \,\mathrm{Re}[\exp(-i\omega t) F_j] \tag{10}$$

and the pressure force due to fluid-loading on the surface of the plate

$$Q_j^p = -\rho c^2 a^2 \,\mathrm{Re}\left[\exp(-i\omega t)\sum_{l=1}^{M} R_{jl} P_l\right] \tag{11}$$

where

$$F_j = \int_{-1/2}^{1/2} f(\xi)\phi_j d\xi \qquad \text{and} \qquad R_{jl} = \int_{-\sigma/2}^{\sigma/2} \phi_j \psi_l d\xi . \tag{12), (13}$$

For a line excitation, $f(\xi)=f\delta(\xi-\xi_e)$, where ξ_e is the location of the force of magnitude f. Combining the Lagrangian equations and the acoustic equations, Eq. (9), a square system of equations is obtained which completely describes the coupled fluid-structure response,

$$\begin{bmatrix} [A] & -2\pi(ka)^2[R]^T \\ [R] & [D] \end{bmatrix} \begin{Bmatrix} P \\ W \end{Bmatrix} = \begin{Bmatrix} \{0\} \\ \{F^e\} \end{Bmatrix} \tag{14}$$

where

$$A_{jl} = \int_{-\frac{\sigma}{2}}^{\frac{\sigma}{2}} \int_{-\frac{\sigma}{2}}^{\frac{\sigma}{2}} \left\{(ka)\psi_j(\xi)\psi_l(\zeta) - \psi_j'(\xi)\psi_l'(\zeta)\right\} \times G(\zeta|\xi) d\zeta d\xi \tag{15}$$

and

$$D_{jk} = \frac{\rho_s h}{\rho a}\left(\left(\frac{c_s}{c}\right)^2 \kappa_{jk} - (ka)^2 \mu_{jk}\right) . \tag{16}$$

The mass per unit surface area of the plate is $\rho_s h$, where h is the plate thickness. The characteristic wave speed for the structure, $c_s=D/\rho_s h a^2$, depends on the bending stiffness of the plate, $D=Eh^3/(12(1-\nu^2))$, where ν is Poisson's ratio. The nondimensional generalized inertia and stiffness coefficients are, respectively,

$$\mu_{jl} = \int_{-1/2}^{1/2} \phi_j \phi_l d\xi \qquad \text{and} \qquad \kappa_{jl} = \int_{-1/2}^{1/2} \phi_j'' \phi_l'' d\xi \ . \tag{17), (18}$$

Once Eq.(14) is solved for the modal coefficients, P_i and W_j, the surface pressure and displacement can be constructed from Eqs. (3) and (5), respectively.

II.2 Formulation for Structural Features

The attached structural features are added to the above formulations by implementation of Hamilton's principle. The displacement of the element is described as some variable, say q_Z. This variable will either be in terms of a main system displacement or be an added degree of freedom which is somehow coupled to the main system motion. Nevertheless, the kinetic, T_f, and potential, V_f, energy expressions for the added feature are combined with the energy expressions for the main system. Of course, for many common features one of these energy relations is not present. A new set of coupled structural equations is obtained when Lagrange's equation is applied to these energy expressions, T_{tot} and V_{tot}. Replacing the original Lagrangian terms, the lower partition of Eq. (14), with the terms that include the added structural features, a new set of equations is obtained which completely describes the behavior of the combined system. Note that some features will increase the number of degrees of freedom of the system by N_Z. Therefore, the size of the system denoted in Eq. (14) will increase accordingly. However, the generalized forces associated with these terms $N+M < i \leq N+M+N_Z$, that is, the added degrees of freedom, will be zero since no external excitation forces are applied to the elements.

III RESEARCH TOPICS AND RESULTS

Determining the effects of feature scales on the structural-acoustic response has not been previously considered in the manner developed here. In this research, scales associated with each structural element, or feature, are introduced into the numerical formulation by describing the element spatial distribution with either an equivalent series expansion or a chapeau function. The influence of different scales on the combined system response is then observed by either changing the number of terms in the series or changing the width of the chapeau distribution.

This research focuses on the influence of inertial, elastic, and coupling scales on the structural-acoustic response of a semi-infinite plate. Inertial and stiffness scale effects are quantified by considering a mass and a spring-suspended mass, respectively. Finally, the scale effects on the coupling of two or more regions of the primary structure are considered by introducing a wave-bearing member supported by spring elements. These structural features are line attachments in that they have an infinite dimension in one direction. Note that in each analysis, only a single subsystem type is considered.

Below is a description of the physical properties and modeling parameters of the bare plate and the acoustic fluid. Then a description of the substructural features considered is presented along with an overview of some results.

III.1 Clean System

The basis functions implemented for the displacement of the plate, Eq. (5), are the orthogonal eigenfunctions for *in vacuo* vibration of a simply supported plate

$$\phi_i = \sin\left[i\pi(\xi + 1/2)\right] \ , \quad -\frac{1}{2} \le \xi \le \frac{1}{2}. \tag{19}$$

with the parameter a set to a value of unity. Likewise, the basis functions for the surface pressure, Eq. (3), are

$$\psi_j = \sin\left[j\pi(\xi/\sigma + 1/2)\right] \ , \quad -\frac{\sigma}{2} \le \xi \le \frac{\sigma}{2} \tag{20}$$

with the baffle size set to a value of $\sigma = 5$. The properties of the steel plate, which is submerged in sea water [5], are

$$a/h = 25, \qquad \rho_s/\rho = 7.58, \qquad c_s/c = 3.84,$$

where h is the thickness of the plate, ρ is the density, c is the wave velocity, and the subscript s refers to steel. Even though coincidence of the plate, ka = 24, is well above the frequency range investigated, acoustic energy will be radiated because of edge affects and anti-symmetries which result from the presence of the substructure.

Convergence of the numerical method can be established by examining the modal amplitudes of the series basis functions for the plate displacement and fluid pressure. For many of the analyses considered in the following section, twenty structural modes, M = 20, and one-hundred fluid modes, N = 100, were used for the range of excitation frequencies considered, 0.05 $\le ka \le$ 10.0. As seen in Figure 2 for two example frequencies, the number of modes used is quite adequate. The magnitudes of the higher numbered coefficients are several orders of magnitude smaller than those with lower indices and are declining with increasing degrees of freedom.

A frequency dependent system parameter commonly used to determine so-called important scales is the free-flexural wavelength given by

$$\frac{\lambda_{ff}}{a} = \frac{2\pi c_f}{\omega}\frac{1}{a}$$

where c_f is the flexural wave speed in the plate ([6], pg. 211). This parameter will be used for comparison purposes in the analyses that follow. For the case at hand, the free-flexural wavelength is that which occurs in an infinite plate with same material properties as those shown above

$$\frac{\lambda_{ff}}{a} = \frac{2\pi}{12^{1/4}}\left(\frac{h}{a}\frac{c_s}{c}\frac{1}{ka}\right)^{1/2} \ . \tag{21}$$

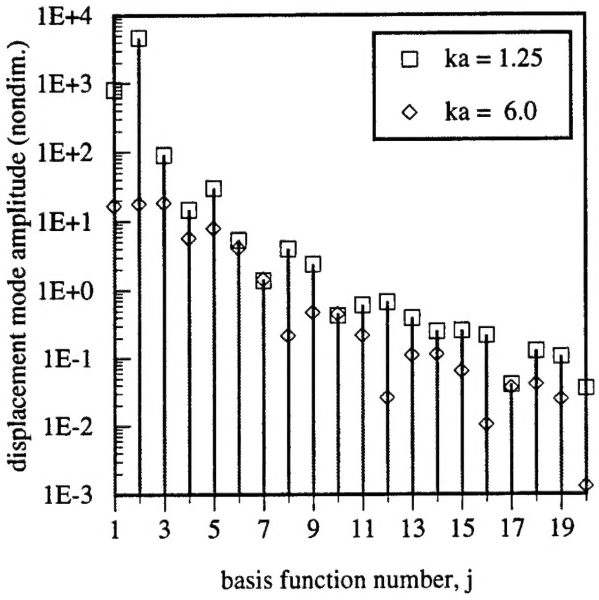

Figure 2a. Convergence of displacement coefficients, $|W_j|$.

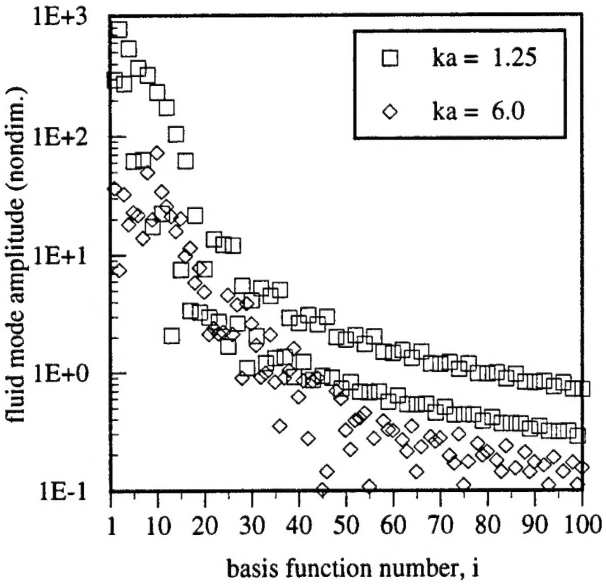

Figure 2b. Convergence of fluid pressure coefficients, $|P_i|$.

III.2 Inertial Scales (Publications 2, 4, 5, 7)*

The effect of inertial scales on the response of the system is the first to be investigated. Inertial scales are analyzed by attaching a line mass to the semi-infinite plate, Figure 3. For the base case the mass is represented using a lumped representation. That is, all of the attached mass is confined to a line parallel to the infinite dimension of the plate. The impact of scales will be studied by comparing the system response for this base case to the response found when the mass is distributed over a certain region of the plate. Two types of distributions, the truncated series and the chapeau function, are considered. The mathematical formulation for these distributions will now be presented.

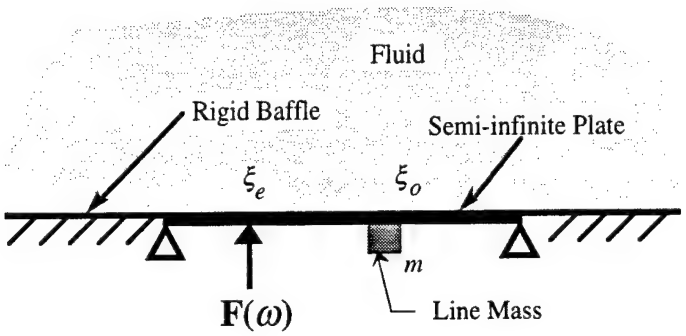

Figure 3. Inertial Scales: Semi-infinite plate with line mass attachment.

As stated above, for the base case, the mass is modeled using a lumped representation

$$m_p(\xi) = m_{rat}\frac{\delta(\xi - \xi_o)}{a} \tag{22}$$

where m_{rat} is the total added mass divided by the plate mass, $m_{rat} = \frac{m_{added}}{\rho_s h a}$, and $\delta(\xi)$ represents the Dirac delta function.

For the first spatial distribution considered, the mass is represented using a sine series spatial expansion,

$$m_s(\xi) = \sum_{n=1}^{L_m} m_n \Gamma_n \tag{23}$$

where L_m is the truncated number of terms and

$$\Gamma_n = \sin\left[n\pi(\xi + 1/2)\right] , \qquad -\tfrac{1}{2} \le \xi \le \tfrac{1}{2}. \tag{24}$$

---

* Publication numbers in ( ) refer to Section VI, items in [ ] refer to reference numbers

Each term in this series represents a certain scale of the distribution. As L_m is increased, the mass becomes more centralized around the attachment position, ξ_o. Conversely, as L_m decreases, the mass becomes more distributed over the plate. Since it is desired to only compare scales, the mass coefficients, m_n, are normalized such that when the value of L_m is changed the total added mass remains constant. Scales are identified as sufficiently small and said to be unimportant when further increase in the number of terms, L_m, resulted in no appreciable change in the predicted system behavior. The mass coefficients are determined from

$$m_n = 2\int_{-\frac{1}{2}}^{\frac{1}{2}} m(\xi)\Gamma_n(\xi)d\xi \quad . \tag{25}$$

Since it is desired to model the point mass using a series, the mass coefficients are found by substituting Eq. (22) into Eq. (25), with the result

$$m_n = 2m_{rat}\sin\left[n\pi(\xi_o + 1/2)\right] \quad . \tag{26}$$

An example series distribution for a single mass located at $\xi = 0.2071$ is shown for a few series lengths, L_m, in Figure 4. Note, that for all the mass examples, the maximum series length is only limited by the necessity of $m/\rho_s ha \geq -1$. Violating this condition results in a non-physical negative mass somewhere along the plate.

Finally, a more uniform mass distribution is considered by implementing a chapeau representation. Denoting the unit step at ξ by $u(\xi)$, the mass can be represented as

$$m_c(\xi) = \frac{m_{rat}}{\Delta_m}\left[u(\xi - (\xi_o - \Delta_m/2)) - u(\xi - (\xi_o + \Delta_m/2))\right] \quad . \tag{27}$$

Instead of changing the series length as above to examine scale affects, the ratio of the mass width to the plate width, Δ_m, is varied. An example for a few distribution widths is shown in Figure 5 for a mass located at $\xi = 0.2071$. As Δ_m decreases the mass becomes more centralized around the attachment position, ξ_o. Conversely, as Δ_m increases the mass becomes more distributed over the plate. Again, since it is desired to only compare scales, when the value of Δ_m is changed the total added mass remains constant.

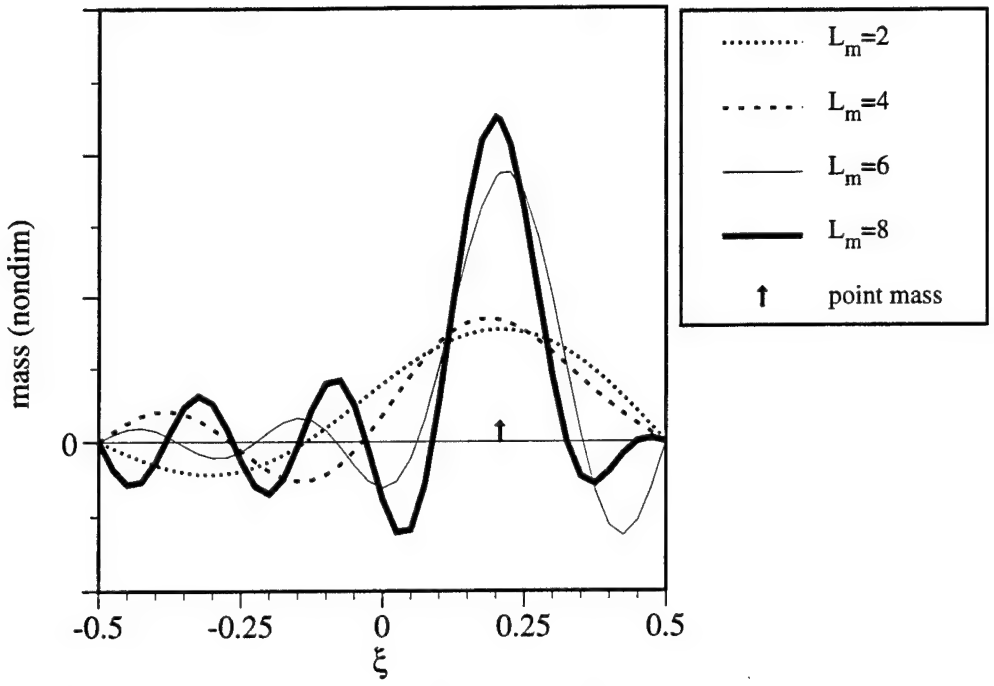

Figure 4. Example mass distribution for finite series.
One mass of 0.25 at $\xi = 0.2071$.

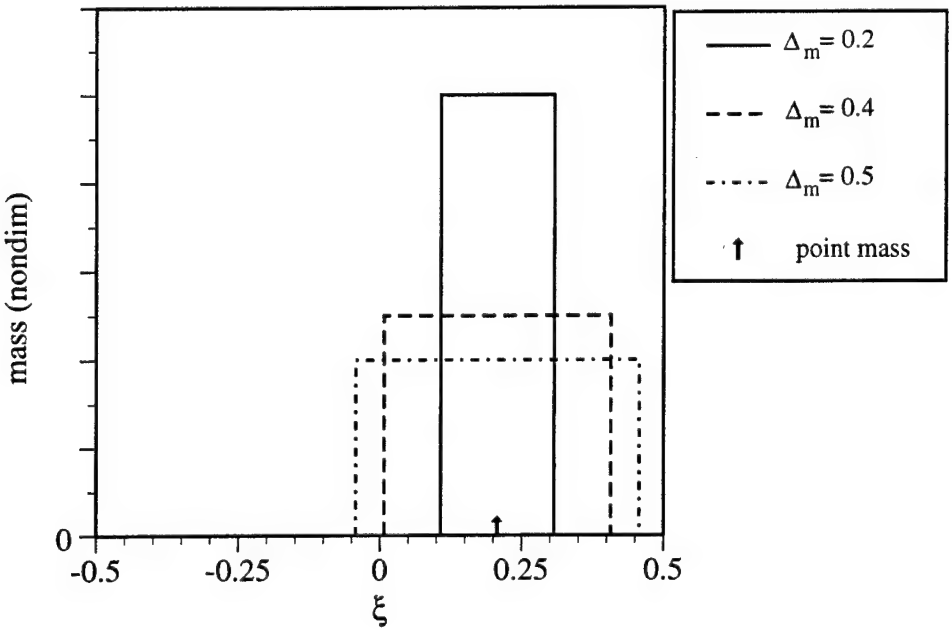

Figure 5. Example mass distribution for chapeau representation.
One mass of 0.25 at $\xi = 0.2071$.

Regardless of the distribution used, the mass is incorporated into the system formulation by determining the nondimensional kinetic energy due to the added mass alone

$$T_m = \frac{1}{2}\frac{\rho_s h}{\rho a}\frac{a^2}{c^2}\sum_{j=1}^{M}\sum_{k=1}^{M}\int_{-\frac{1}{2}}^{\frac{1}{2}} m(\xi)\,\phi_j\,\phi_k\,d\xi\,\dot{q}_j\dot{q}_k \quad . \tag{28}$$

Recall that $m(\xi)$ is relative to the plate mass in Eqs. (22), (26), and (27). After applying Lagrange's equations, the relation for D_{jk}, Eq. (16), is modified as

$$D_{jk}^{m} = \frac{\rho_s h}{\rho a}\left(\left(\frac{c_s}{c}\right)^2 \kappa_{jk} - (ka)^2 \mu_{jk} - (ka)^2 \eta_{jk}\right) \tag{29}$$

where the inertial coupling coefficient, η_{jk}, depends on the type of distribution used. When the lumped representation Eq. (22) is used

$$\eta_{jk} = m_{rat}\,\phi_j(\xi_o)\,\phi_k(\xi_o) \quad . \tag{30}$$

For the series representation Eq. (23), however, it is defined as

$$\eta_{jk} = \int_{-1/2}^{1/2}\sum_{n=1}^{L_m} m_n\,\Gamma_n\,\phi_j\,\phi_k\,d\xi \quad . \tag{31}$$

And finally, for the chapeau distribution, Eq. (27), the inertial coupling coefficient becomes

$$\eta_{jk} = \frac{m_{rat}}{\Delta_m}\int_{\xi_o-\Delta_m}^{\xi_o+\Delta_m} \phi_j\,\phi_k\,d\xi \quad . \tag{32}$$

The inertial coupling coefficient is named such because as expressed in Eq. (31), for example, it can be used to investigate the coupling of inertial scales in the substructure to scales in the main structure.

The forced response of the combined system can now be predicted using Eq. (14) provided D_{jk} is replaced by D_{jk}^{m}. It should be noted that in the formulation presented here the distributed mass is treated as a locally reacting structure in that it can only exert forces normal to the surface of the plate. In other words, the mass does not react to bending forces.

Several metrics could be used to determine the effects of the mass distribution. Plate surface displacement, surface velocity, surface pressure, and far-field directivity are just a few characteristics that could be studied. However, a single number metric which gives a good indication of changes to the system response is the radiated acoustic power. For the work presented here, the power radiated with a distributed mass, Eq. (23) or (27), will be compared to

the power radiated using a lumped mass representation, Eq. (22). It will also prove convenient to represent the change in power as the logarithmic difference in the power for the distributed mass and the power for the lumped mass, that is,

$$\Delta \text{Power} = 10 \log_{10} \left(\frac{\text{Power}_{distributed}}{\text{Power}_{lumped}} \right) . \tag{33}$$

Consider the case of a line mass of m_{rat} = 0.25 attached to the plate at ξ = 0.2071. The system is harmonically excited by a line force located at ξ_e = -0.25. With the mass in a lumped configuration, the first three fluid-loaded resonances for this case occur at approximately $k_1 a$ = 0.2, $k_2 a$ = 1.25, and $k_3 a$ = 3.35. The change in the radiated power due to using the series representation instead of a lumped representation is shown in Figure 6. First note that while used for illustrative purposes, the lines are not continuous in the L_m direction. That is, a series length of five and one-half is not possible. Also note that the maximum series length for this configuration is L_m = 16. As expected, the effects of the distribution on the change in radiated power are most drastic around the resonances. However, the radiated power around the first resonance is basically not affected by using a series distribution in that the differences in radiated power for all series lengths considered are much less than 1 dB. Therefore, only the data around the second and third of these frequencies is shown. Near the second resonance, the lower series lengths can give as much as a 6 dB error in predicting the radiated power. The behavior of the contour lines is due to the shifting of the resonance peaks caused by distributing the mass. Although the total added mass does not change, the changing distribution causes the resonance frequency to slightly change thus resulting in a large change in the radiated power at a particular frequency. For all of the frequencies considered, eight terms was the most needed to get an accurate prediction of the radiated acoustic power. Therefore, for the series distribution, inertial scales associated with terms nine and higher do not cause a noticeable impact on the radiated power at a particular frequency.

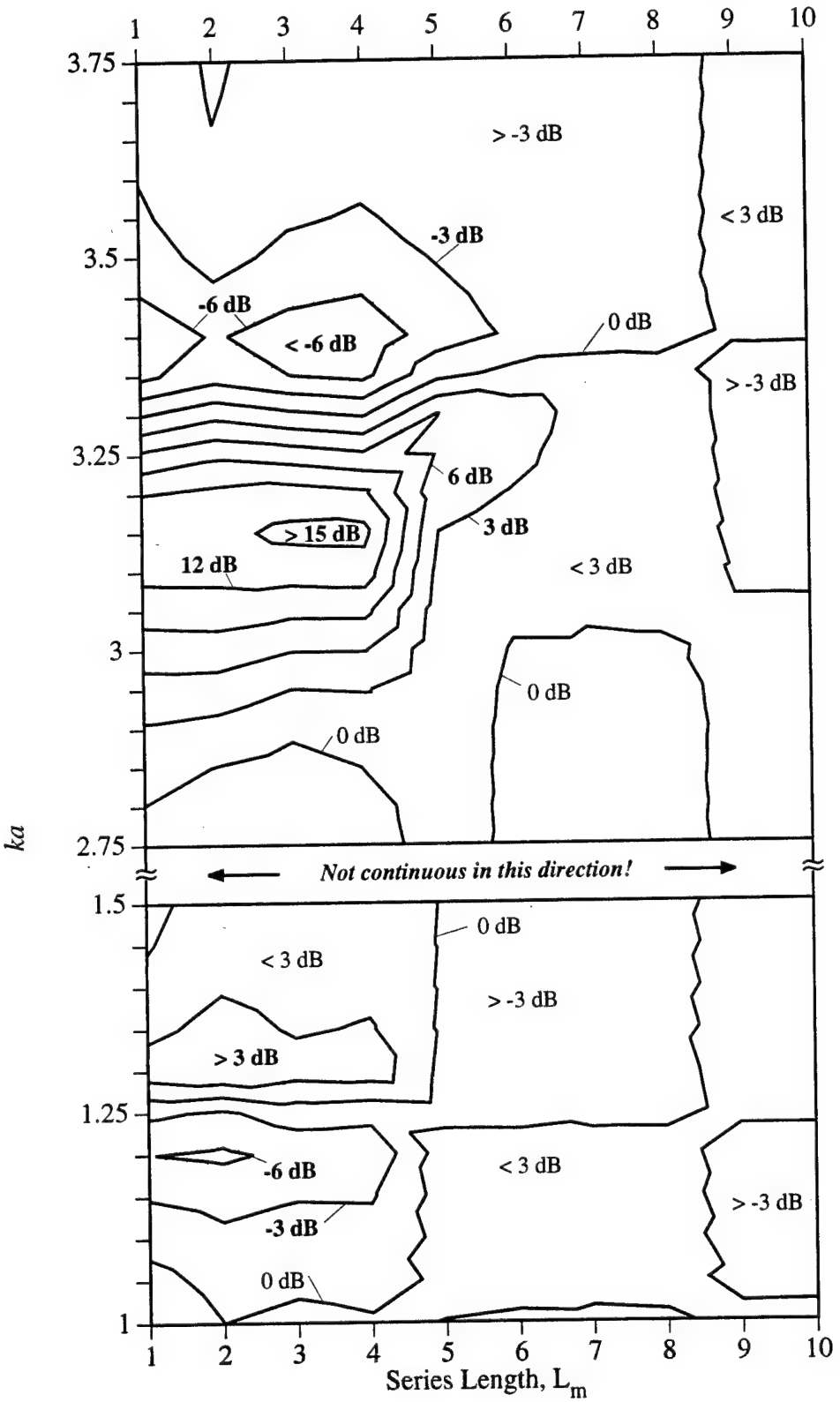

Figure 6. Change in radiated power due to representing a lumped mass with a series representation. One mass of $m_{rat} = 0.25$ located at $\xi = 0.2071$.

Before considering the next type of distribution it is interesting to note one more attribute of the series representation. In general, when approximating an impulse function with a finite series, adding more terms improves the approximation. When predicting the radiated acoustic power, however, increasing the number of spatial series terms does not always guarantee a solution that more closely matches that of the lumped mass. For example, consider the case of four masses of 0.1 each that are equally spaced along the plate span. Figure 7 shows a comparison of the radiated power predicted using the series representation to that predicted using a lumped mass representation. It can be seen that at ka = 3.2 series lengths of 7 and 8 give results closer to the lumped model than lengths of 6, 9, and 10. For the single mass case, the same type of behavior occurs in Figure 6 around ka = 3.15 for the smaller series lengths.

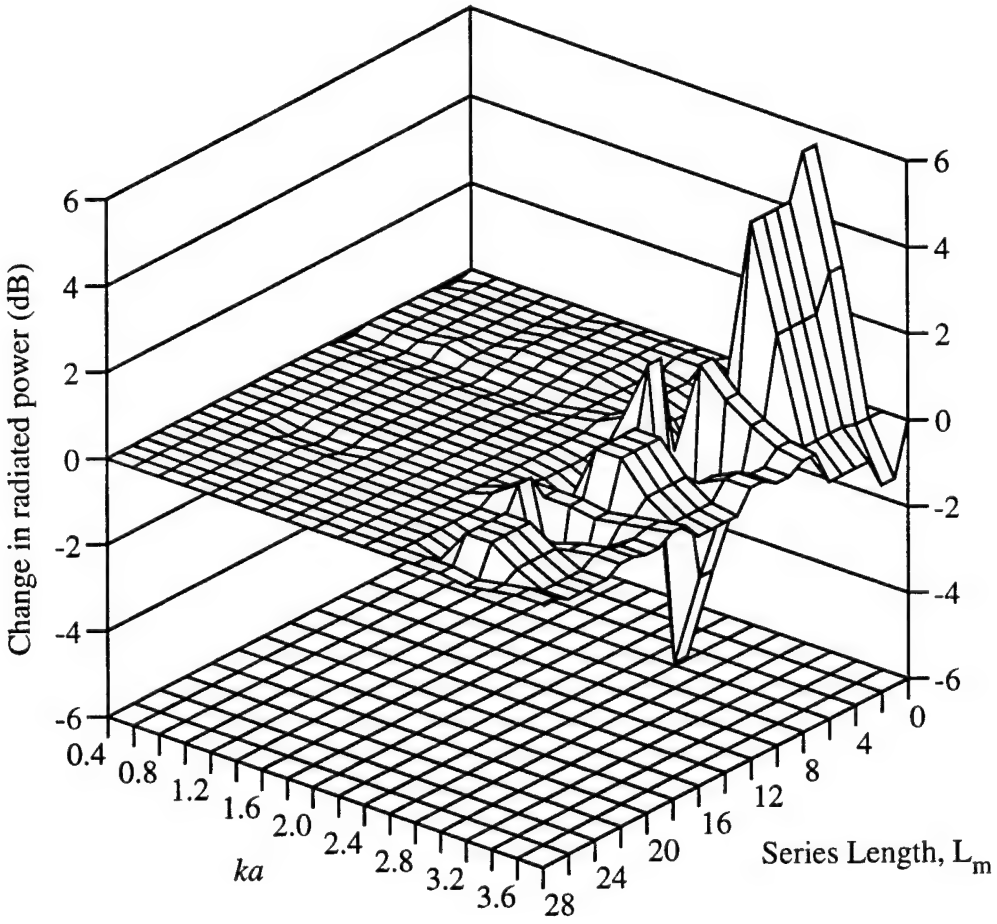

Figure 7. Change in radiated power for various series lengths, L_m.
Four equally space masses of 0.1 each. Lumped case = 0 dB.

A comparison of the radiated power found using the lumped mass to the power found using a chapeau mass distribution, Eq. (27), is shown in Figure 8. Again, the mass of $m_{rat} = 0.25$ is located at $\xi = 0.2071$ and the excitation is at $\xi_e = -0.25$. The lines in this figure represent constant multiples of ± 3 dB. Due to the placement of the mass at $\xi = 0.2071$, the maximum distribution width is about $\Delta_m = 0.58$. As expected, most of the impact due to scales occurs around fluid-loaded resonances. Also shown in the figure is a dashed line representing the percent of the plate span that would be occupied by one-quarter of a free-flexural wavelength at the excitation frequency. A features size is often considered to be unimportant when its characteristic dimension is smaller than one-quarter of a free-flexural wavelength, $\lambda_{ff}/4$. As can be seen in the figure, however, inertial scales less than $\lambda_{ff}/4a$ can be very important. Near the third resonance, at $ka = 3.25$, for example, using a lumped representation to model a mass that is actually distributed over 15% of the plate span, or $\Delta_m = 0.15$, can result in under predicting the radiated acoustic power by almost 6 dB. However, when the forcing is at a single frequency away from the resonances, any mass distribution considered, including the lumped representation, can be used to predict the acoustic power to within less than ± 3 dB of error.

As a result, for the frequency range considered, inertial scales of less than one-eighth of the plate span are not important. For most of the frequency range, when a representation is used, Eqs. (23) or (27), such that most of the mass is confined to a region of less than one-eighth of the plate span, scales no longer become important. Therefore, whenever the mass distribution is confined to within this region, a lumped mass representation may be used without significantly affecting the predicted acoustic behavior. When a broadband excitation for $0.5 \leq ka \leq 4.0$ is applied to the system the change in radiated power is much larger, Figure 9. This plot is somewhat crude in the sense that it is simply a sum of the ka data points in Figure 7 which are spaced at increments of 0.05. Therefore, if all of the frequencies were present in the actual excitation, then the error may be somewhat different. However, it would then be necessary to perform an integration under the curve to obtain accurate values. Nevertheless, as can be seen from this plot, an error of more than 3 dB is attained when the mass is distributed over more than one eighth of the plate or $\Delta_m > 0.12$.

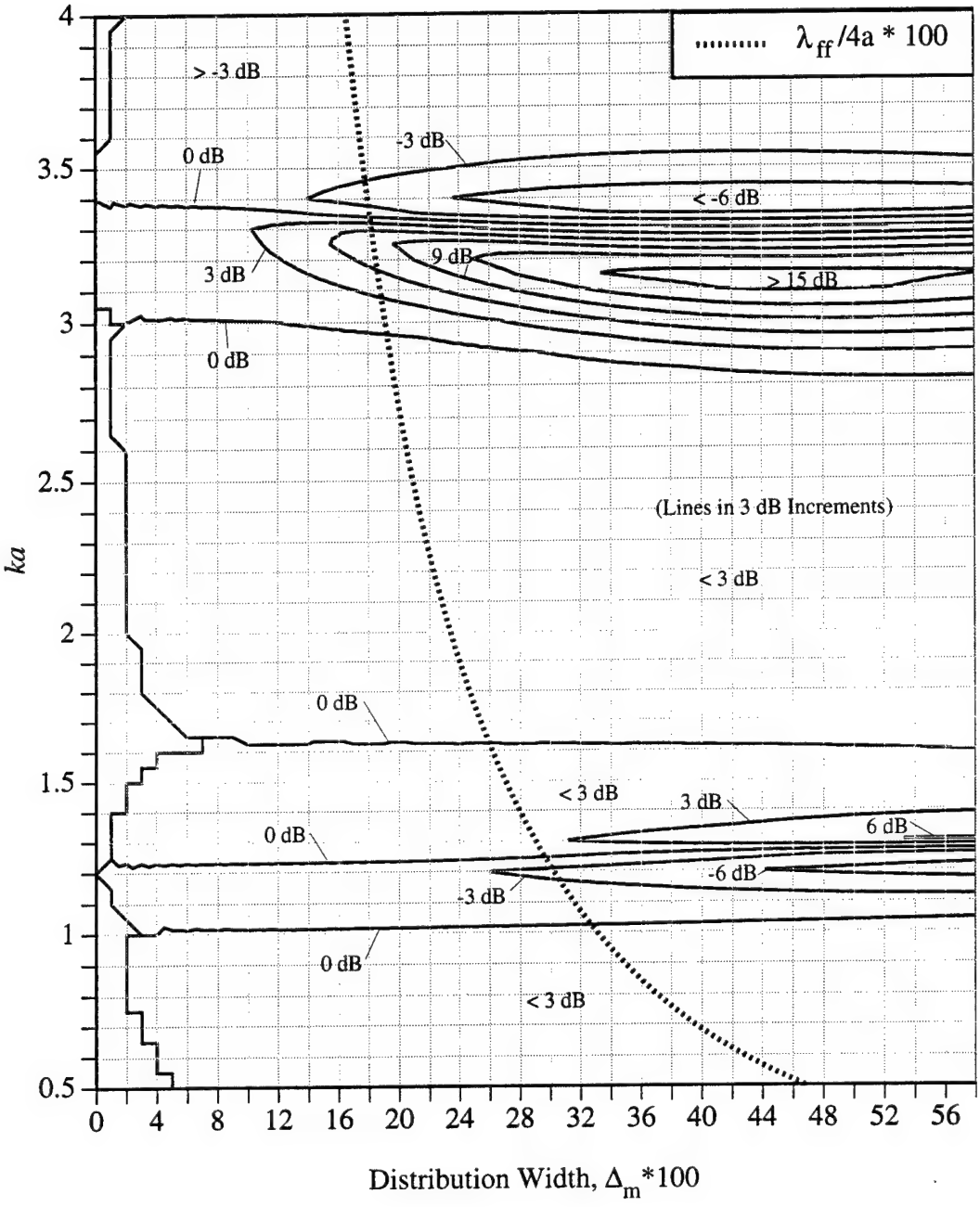

Figure 8. Change in radiated power due to treating a distributed mass as a lumped mass. One mass of $m_{rat} = 0.25$ located at $\xi = 0.20711$

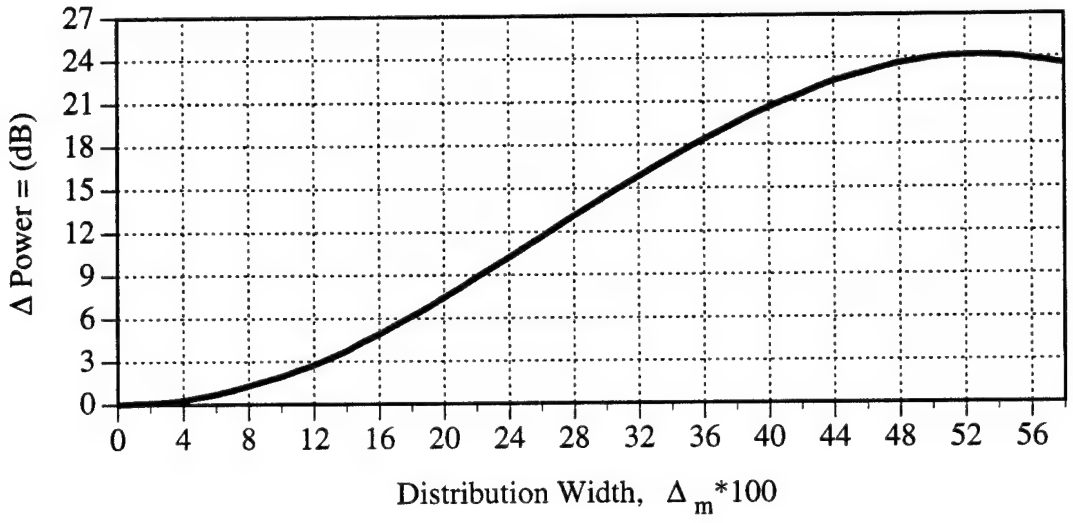

Figure 9. Change in radiated power due to treating a distributed mass as a lumped mass. One mass of $m_{rat} = 0.25$ at $\xi = 0.2071$. Broadband excitation $0.5 \leq ka \leq 4.0$ in 0.05 increments.

III.3 Elastic Scales (Publications 3, 9)

Next the impact of elastic scales on the structural acoustic response of the system is considered. Here it is desired to determine the influence of stiffness distributions at different spatial scales. To that end, consider a line mass attached to the plate by a line spring at a position ξ_o, Figure 10. Note that the number of degrees of freedom of the system increases by one due to the added spring/mass. The types of distributions used are the same as those used for the mass described above. The suspended mass, however, is represented as a lumped element throughout this analysis.

The representation for a lumped spring located at ξ_o is

$$k_p(\xi) = k_{rat} \frac{\delta(\xi - \xi_o)}{a} \tag{34}$$

where k_{rat} is the stiffness of the added spring, k_A, divided by the bending stiffness of the plate, or, $k_{rat} = \dfrac{k_A a^2}{D}$.

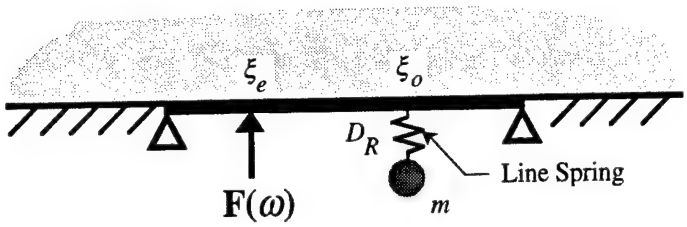

Figure 10. Elastic Scales: Semi-infinite plate with Line mass suspended by line spring.

In the exact manner as above, the spatial series representation for the spring is given by

$$k_s(\xi) = \sum_{n=1}^{L_s} k_n \Gamma_n \tag{35}$$

where L_S is a truncated number of terms and Γ_n is given in Eq. (24). The number of terms in the expansion will be varied to study scale effects. The stiffness coefficients, k_n, are calculated in exactly the same manner as for the mass distribution in Eq. (25).

Denoting the unit step at ξ_o by $u(\xi\text{-}\xi_o)$, the stiffness distribution can also be represented with a chapeau distribution as

$$k_c(\xi) = \frac{k_{rat}}{\Delta_k}[u(\xi - (\xi_o - \Delta_k / 2)) - u(\xi - (\xi_o + \Delta_k / 2))] \tag{36}$$

where the width of the distribution is Δ_k. To examine scale effects of the stiffness, the width of the distribution, Δ_k is varied. With each Δ_k , however, the total added stiffness remains constant.

The system of equations given by Eq. (14) must now be modified to account for the added subsystem since the number of degrees of system is increased by N_Z = 1. Defining the extra degree of freedom as q_z, the potential energy of the added spring is

$$V_k = \frac{1}{2}\frac{D}{a}\left\{\sum_{j=1}^{M}\sum_{k=1}^{M}\alpha_{jk}^{A} q_j q_k - 2\sum_{j=1}^{M}\alpha_j^{B} q_j q_z + \alpha_z^{C} q_z q_z\right\} \tag{37}$$

where the stiffness coupling coefficients are defined as

$$\alpha_{jk}^{A} = \int_{-\frac{1}{2}}^{\frac{1}{2}} k(\xi)\phi_j(\xi)\phi_k(\xi)d\xi, \qquad \alpha_j^{B} = \int_{-\frac{1}{2}}^{\frac{1}{2}} k(\xi)\phi_j(\xi)d\xi, \tag{38), (39}$$

and

$$\alpha_z^C = \int_{-\frac{1}{2}}^{\frac{1}{2}} k(\xi)\, d\xi \quad . \tag{40}$$

When solving for the lumped element solution, $k(\xi)$ in the above equations is replaced by $k_p(\xi)$. Similarly, $k_s(\xi)$ and $k_c(\xi)$ are substituted to determine the coupling coefficients for the series and chapeau distributions, respectively.

The added kinetic energy term due to the mass is found by modifying Eq. (28). Since the mass is now affixed to the added degree of freedom q_z, the terms $\dot{q}_j$ and $\dot{q}_k$ are each replaced by $\dot{q}_z$ and M is replaced by $N_Z = 1$

$$T_{\hat{m}} = \frac{1}{2}\frac{\rho_s h}{\rho a}\frac{a^2}{c^2}\hat{m}_{rat}\,\dot{q}_z\dot{q}_z = -\frac{1}{2}\frac{\rho_s h}{\rho a}\frac{(ka)^2}{c^2}\hat{m}_{rat}\,q_z^2 \tag{41}$$

Numerical modeling problems can occur when using the series representation, Eq. (35), for the elasticity. Unlike the chapeau distribution, a series can result in a locally negative potential energy for the combined system near the edges of the plate. This is due to the fact that the series representation takes on negative as well as positive values. Since the potential energy of the plate alone gets small near the baffle, the combined system potential energy can have a negative value near the edges of the plate. This occurs even though the total system potential energy is still positive. The result is a localized negative elasticity. This numerical problem is analogous to having a locally negative mass in the preceding section, that is $m/\rho_s ha < -1$. However, the condition here is violated for many stiffness values of interest. Therefore, to avoid problems associated with this irregularity, the series representation is not used to model the spring.

It should again be noted that in the foregoing analyses the distributed elements are treated like a locally reacting components. That is, only normal forces can be exerted on the plate by the distributed elasticity.

After applying Lagrange's equations, the relation for D_{jk}, Eq. (16), is modified as

$$D_{jk}^s = \frac{\rho_s h}{\rho a}\left(\left(\frac{c_s}{c}\right)^2 \kappa_{jk} - (ka)^2 \mu_{jk} + \left(\frac{c_s}{c}\right)^2 \alpha_{jk}^A\right) \quad . \tag{42}$$

Since there is an increase in the number of degrees of freedom, Eq. (14) is no longer valid. The matrix of equations describing the combined system is now

$$\begin{bmatrix} [A] & -2\pi(ka)^2[R]^T & [0] \\ [R] & [D^S] & [K]^T \\ [0] & [K] & [M] \end{bmatrix} \begin{Bmatrix} P \\ W \\ Z \end{Bmatrix} = \begin{Bmatrix} \{0\} \\ \{F^e\} \\ \{0\} \end{Bmatrix} \tag{43}$$

where

$$K_j = -\frac{\rho_s h}{\rho a}\left(\frac{c_s}{c}\right)^2 \alpha_j^B, \tag{44}$$

and

$$M_j = \frac{\rho_s h}{\rho a}\left[\left(\frac{c_s}{c}\right)^2 \alpha_z^C - (ka)^2 \hat{m}_{rat}\right], \tag{45}$$

and the lumped mass is designated by $\hat{m}_{rat}$.

Consider an added line mass of $\hat{m}_{rat} = 0.25$ suspended by an added line stiffness of $k_{rat} = 2860.0$ at $\xi = 0.2071$ with the harmonic force excitation at $\xi_e = -0.25$. These mass and stiffness values correspond to a *in vacuo* vibration absorber tuned to $ka = 5.0$. Within the frequency range considered, the in-fluid resonances of the combined system with a lumped spring are approximately $ka = 0.2$, 1.25, and 3.35. Similar to the mass analysis above, the power radiated with a distributed stiffness, Eq. (36), will be compared to the power radiated using a lumped spring representation, Eq. (34).

The radiated acoustic power versus frequency is shown for the lumped spring as well as several distributed stiffnesses of a chapeau representation in Figure 11. The power appears to vary the most from the lumped representation solution at and around the in-fluid resonances, which are marked on the figure. For a more direct comparison, the change in the acoustic power is shown in Figure 12. Although the largest differences do occur at the resonances, large differences also occur between resonances. For example, at $ka = 3.0$, a spring which is distributed over less than one-quarter (22%) of the plate span will result in a radiated power which is 3 dB greater than that which would be predicted when using a lumped element representation. This occurs even though, on a local scale, the local stiffness is smaller for larger distribution widths. For the type of distribution used, though, when the excitation frequency is between resonances, stiffness scales less than ten percent of the plate span may be represented as lumped elements without any significant change in the predicted acoustic power .

Figure 13 shows lines of constant change in radiated power versus nondimensional frequency, ka, and distribution width, Δ_k. For clarity, only the lines separating the regions of 0 dB, less than -3 dB, and greater than + 3 dB are shown. Note that since the spring-mass subsystem is located at $\xi = 0.2071$, the maximum distribution width allowed is approximately 58% of the span. If this width is exceeded, the center of the spring must be relocated to avoid

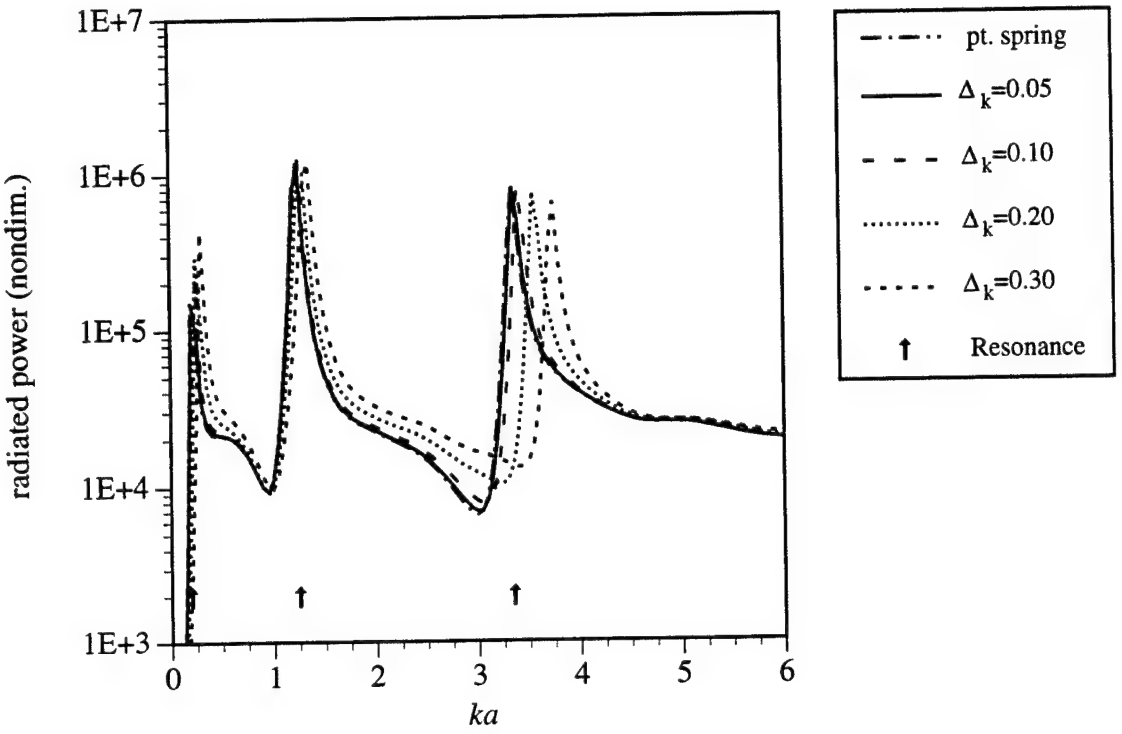

Figure 11. Radiated acoustic power for a lumped element and various distribution widths, Δ_k. $k_{rat} = 2860$.

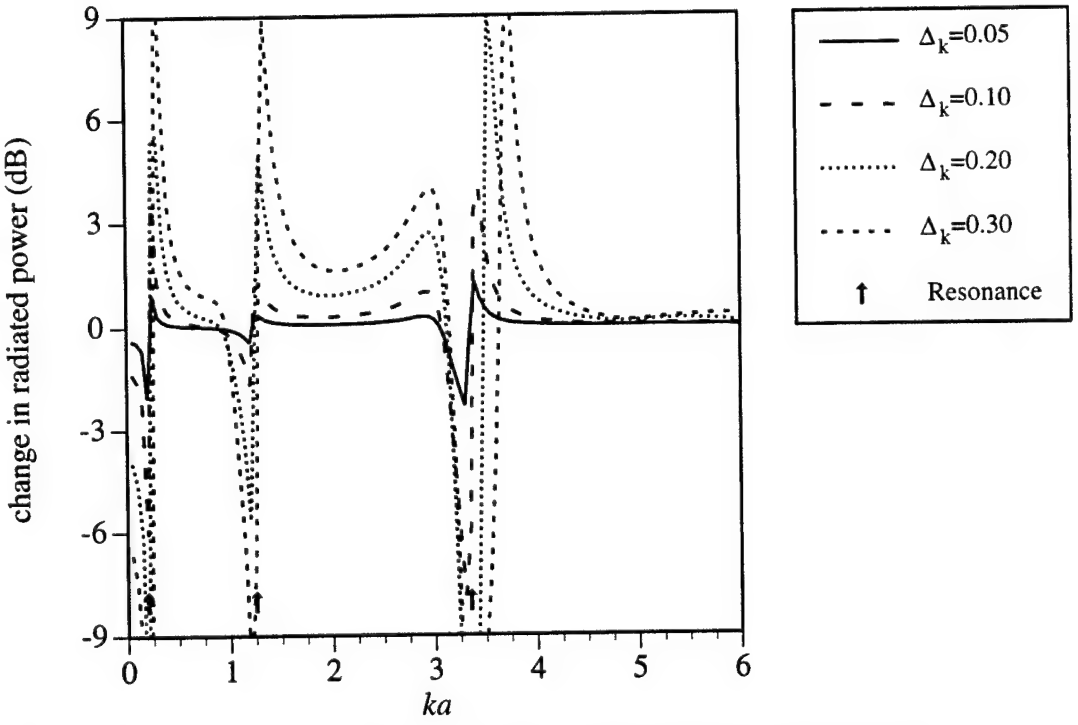

Figure 12. Increase in predicted power using a stiffness distribution of width Δ_k instead of a lumped element. $k_{rat} = 2860$.

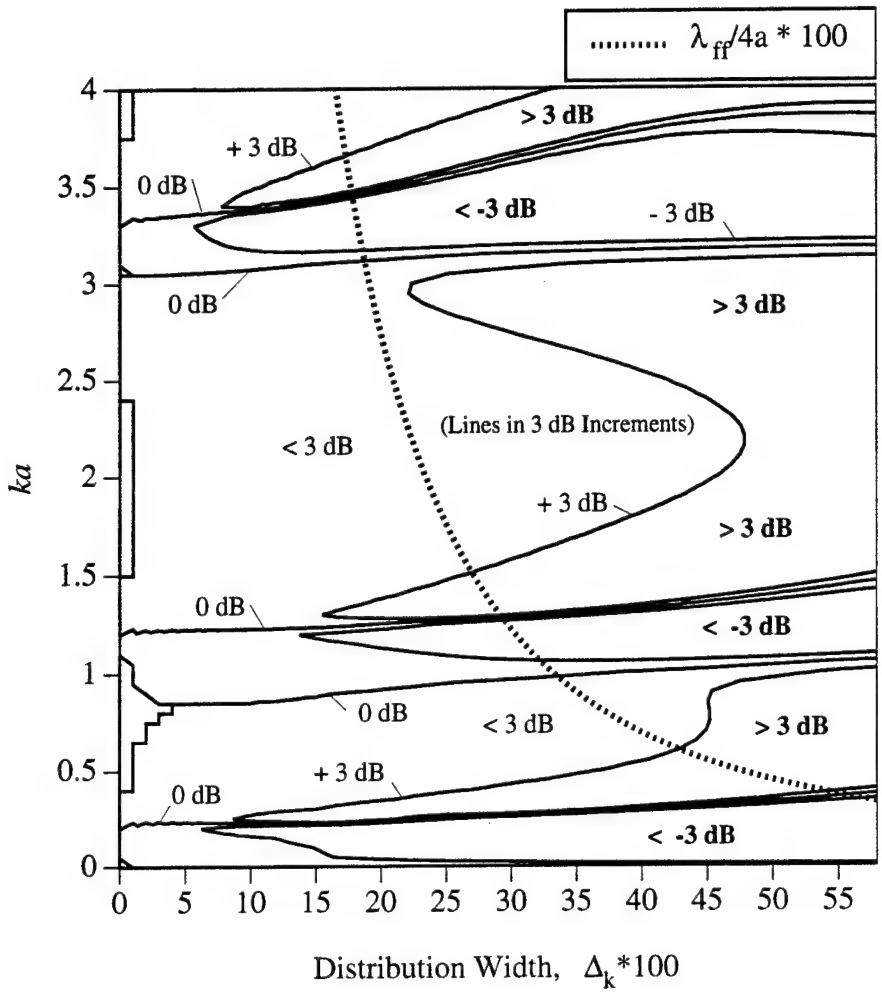

Figure 13. Difference in radiated power between distributed and lumped representations as a function of wavenumber, *ka*, and distribution width, Δ_k. k_{rat} = 2860.

distributing the stiffness over the baffle. Figure 13 clearly shows that over much of the *ka* range considered, a feature spanning 10 to 15% of the plate span may be modeled as a lumped element while introducing only a small error in the predicted acoustic power. Figure 13 also indicates that the greatest difference between the lumped and distributed representations is near the fluid-loaded resonances, with the region of affected *ka* values broadening as the feature scale increases. For an infinite plate with the same physical properties as those used here, the free-flexural wavelength has a value of 0.66*a* at *ka* = 4.0. Therefore, depending on the degree of precision desired in the numerical simulation, Figure 13 indicates that elastic scales less than one-quarter of a flexural wavelength can be important. For example, at *ka* = 1.3 the free-flexural

wavelength is $1.16a$. A distribution width of one-fifth of a free-flexural wavelength at this frequency is around 23% of the plate span or $\Delta_k = 0.23$. As shown in the figure, using a lumped element to represent this spring would result in under predicting the radiated acoustic power by more than 3 dB. Over a majority of the *ka* range considered, however, elastic scales less than 10% of the free-flexural wavelength can be modeled using a lumped element representation without any significant penalty to the numerical prediction.

For the examples shown, elastic scales less than one-tenth of the main structure dimensions can be replaced with the much simpler lumped element representation without significantly affecting the numerical prediction.

III.4 Coupling Scales: Subplate - Spring Subsystem (Publication 8)

The final subsystem to be considered for the plate is a semi-infinite plate, referred to hereafter as a subplate, suspended by a line spring at each edge, Figure 14. The springs are modeled using the series method described in the previous section. The motion of the suspended plate, however, is treated using a modal expansion with a fixed number of terms. For the sake of brevity, only the modeling of the subplate will be described. The motion of the subplate is described using the expansion,

$$z(\zeta,t) = \sum_{i=1}^{M_p} \Omega_i(\zeta) q_i^z(t) \tag{46}$$

where M_P is the truncated number of assumed modes, q^z are the modal amplitudes, that is, the extra degrees of freedom, and ζ is the nondimensional coordinate of the subplate. The basis functions used for the subplate displacement are the normalized orthogonal free-free modes [7]

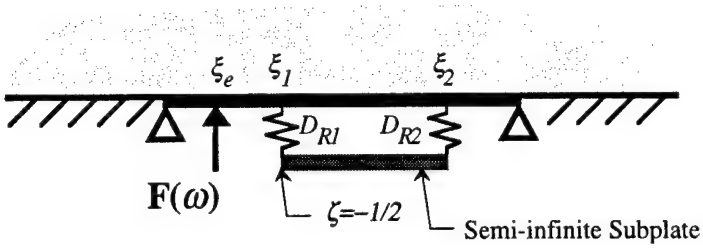

Figure 14. Coupling Scales: Semi-infinite wave-bearing subplate suspended by line springs

given as

$$\Omega_0(\zeta)=1, \qquad -1/2 \le \zeta \le 1/2$$

$$\Omega_1(\zeta)=\sqrt{3}(\zeta) \tag{47}$$

$$\Omega_i(\zeta)=\cos(\beta_i(\zeta+1/2))+\cosh(\beta_i(\zeta+1/2)) \\ -C(\sin(\beta_i(\zeta+1/2))+\sinh(\beta_i(\zeta+1/2))) \qquad , \quad i\ge 2 \ .$$

$$C=\frac{\cos(\beta_i)-\cosh(\beta_i)}{\sin(\beta_i)-\sinh(\beta_i)}$$

The values of β_i are the solutions to the eigenvalue equation, $\cos\beta_i \cosh\beta_i = 1$, noting that $\beta_0 = \beta_1 = 0$. The functions Ω_0 and Ω_1 in Eq. (47) are for pure translation and pure rotation, respectively, of the subplate.

While the springs may be distributed over the main plate, they are only attached to the endpoints of the subplate. As a result, the potential energy expressions for each of the springs are the same as Eq. (37) provided that q_z is replaced by $Z(\zeta_o=\pm 1/2)$, depending on the spring being considered. That is, Eqs. (38)-(40) become

$$\alpha_{jk}^{A}=\int_{-\frac{1}{2}}^{\frac{1}{2}}\sum_{n=1}^{L_s} k_n \Gamma_n \phi_j \phi_k \, d\xi , \qquad \alpha_{jl}^{B}=\int_{-\frac{1}{2}}^{\frac{1}{2}}\sum_{n=1}^{L_s} k_n \Gamma_n \phi_j \, d\xi \, \Omega_l(\zeta_0), \tag{48), (49}$$

and

$$\alpha_{jk}^{C}=\int_{-\frac{1}{2}}^{\frac{1}{2}}\sum_{n=1}^{L_s} k_n \Gamma_n \, d\xi \, \Omega_j(\zeta_0)\Omega_k(\zeta_0) \ . \tag{50}$$

The kinetic and potential energy expressions for the subplate are similar to those for the main plate [2] except the new modal functions, Ω, and the physical properties of the subplate are used. Taking into account these modifications, the system is then be solved using Eq. (43). The resulting $\boldsymbol{Z}$ vector provides the modal amplitudes of the series expansion, Eq. (46), used to construct the structural motion of the subplate. It should be pointed out that the number of subplate modes, M_P, will not be changed once convergence has been verified.

The harmonic force excitation is located at ξ_e = -0.25 and the range of forcing frequencies considered is $0.05 \le ka \le 6.0$. The properties of the subplate are

a_p/a=0.5, ρ_p/ρ_s = 0.3506, c_p/c_s = 1.0, and h_p/h=1.426

where the subscript p refers to the subplate. These properties roughly correspond to a subplate with a density equal to that of aluminum and a mass equal to one-quarter that of the main plate. The subplate motion is described using an M_p = 12 mode expansion.

For a sample case, the subplate is suspended by springs located at ξ = -0.293 and ξ = 0.207. An example of the stiffness distribution for various series lengths is shown in Figure 15. Again, the total stiffness is the same for all of the expansions.

For the first example, the springs have a stiffness ratio of $k_{rat1} = k_{rat2}$ = 12.17. Here the series expansion can be implemented because the added stiffness values are much lower than in the preceding section. The power radiated with the distributed stiffness is compared to the power radiated using the lumped spring representations in Figure 16. For example, at ka = 0.25, a spring which is distributed using a four term expansion will result in a radiated power which is about 1 dB greater than that which would be predicted using a lumped element representation. Since the differences are small above ka = 2.0, frequencies above that value are not shown. As before, simply increasing the number of terms does not guarantee a better prediction. As expected, the largest differences occurs near the resonances. Increasing the value of the spring stiffnesses to $k_{rat1} = k_{rat2}$ = 17.17 has the affect of amplifying these differences in power near the resonances as shown in Figure 17. Away from the resonances, however, the effect is not as noticeable. The resonances associated with lumped springs are indicated in the figures. Note that around ka = 0.5 the distribution caused an increase in the power for the larger stiffness while

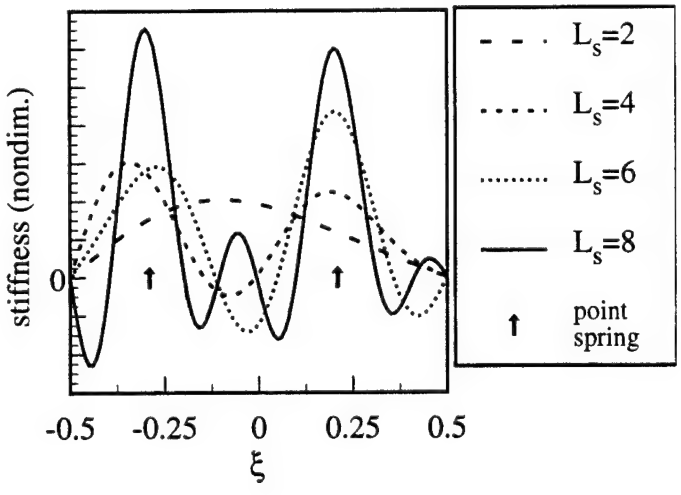

Figure 15. Example stiffness distribution for various series lengths, L_S.

causing a decrease for the smaller stiffness. For the stiffness values given in this example, though, when the excitation frequency is between resonances, all of the stiffness scales shown may be represented as lumped elements without any significant change in the predicted acoustic power. These changes become larger when higher valued stiffnesses are used. However, the numerical problems associated with negative elasticity, mentioned in the previous section, can become more of a concern. Results for this analysis using the chapeau distribution have not been obtained at this point in the research.

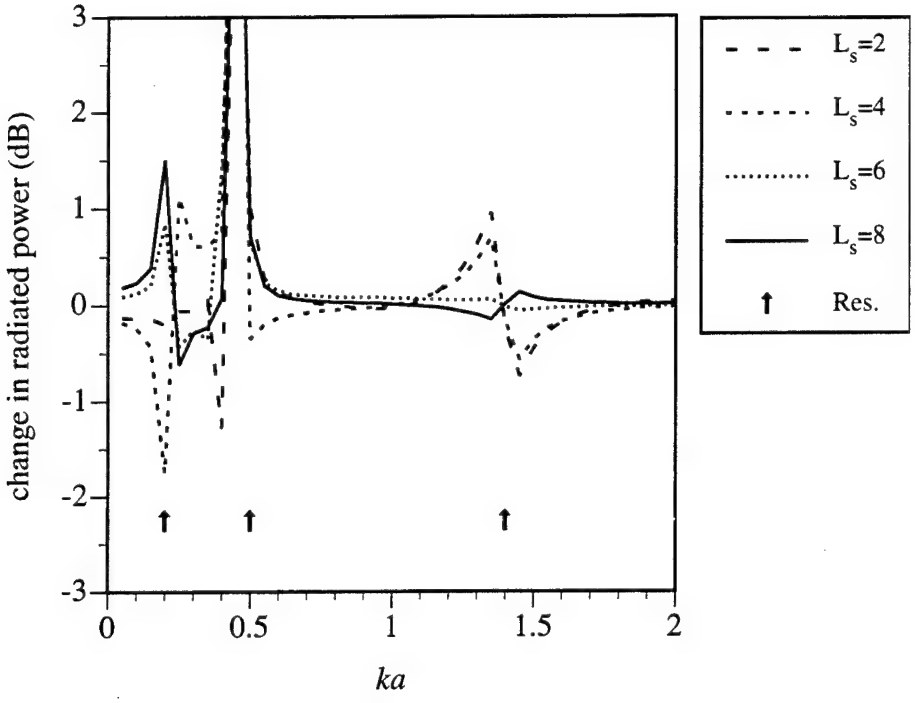

Figure 16. Change in radiated power for various series lengths, L_S.
$D_{Rtot} = 24.34$

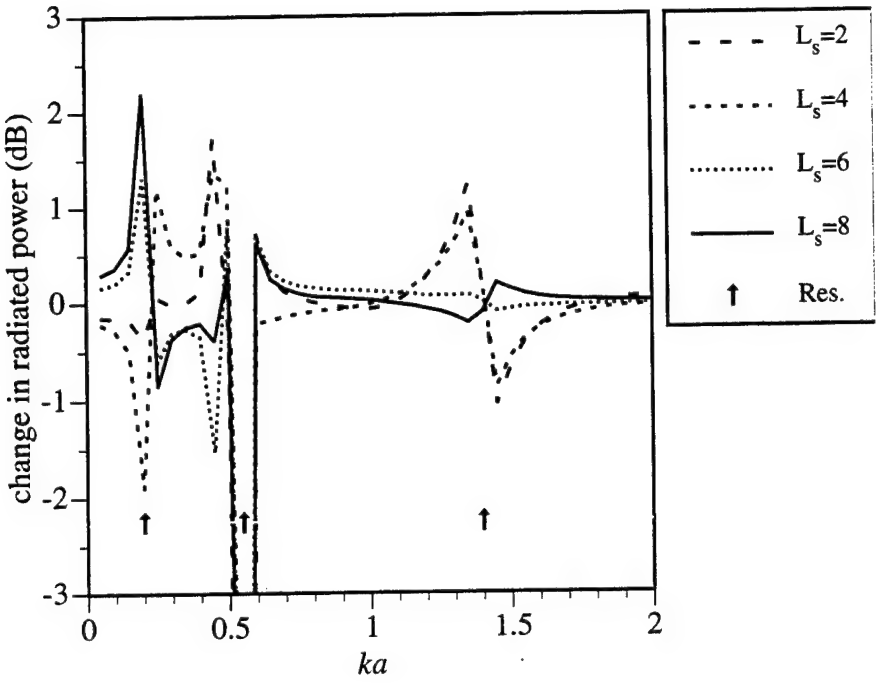

Figure 17. Change in radiated power for various series lengths, L_S.
D_{Rtot} = 34.34

IV. MODELING OF CYLINDRICAL SHELL STRUCTURES

The primary thrust of this work was to extend the surface variational principle (SVP) to capped cylindrical shells. Prior development of SVP for axisymmetric shapes had only considered axisymmetric excitations in the form of an oscillatory force. The SVP formulation is the only modeling technique that represents the surface response in a spectral manner. Thus, extending the scales formulation to treat phenomena encountered in cylindrical shell structures required prior work advancing the generality of the technique. Equally important, it was deemed essential that all work be verified by comparison with accepted structural acoustics boundary element or finite element computer codes.

The first phase of this effort entailed modifying the basic variational principle to address scattering problems. This was achieved by rederiving the principle from a seldom used version of the Kirchhoff-Helmholtz integral theorem, in which the scattered pressure (rather than the total pressure) is the basic variable. The computer programs were correspondingly altered. The results obtained from these programs for end-on scattering from flat and hemi-capped rigid

cylinders were verified by comparing surface pressures with those obtained from the CHIEF program.

The next effort was devoted to implementing SVP for situations where the surface response is not axially symmetric. This was achieved by using an azimuthal harmonic decomposition in which each succeeding harmonic is obtained in a semi-recursive manner from previously computed harmonics. Although only rigid body configurations were considered here, the analyses considered both arbitrary types of rigid body motion, and scattering of waves at arbitrary incidence to rigid bodies. Here again, CHIEF was used to verify the results.

The final effort involved coupling the general version of SVP with a structural dynamics formulation, in order to address the ultimate objective of submerged shells. Because the overall project needed to avoid modeling techniques entailing discretized representations of the structural motion, a new formulation for vibrations of axisymmetric shells was developed. The technique uses a Ritz series expansion of the meridional variation of displacement, coupled with a Fourier decomposition of the azimuthal dependence. The unique aspect of the formulation is the method by which the meridional basis functions are selected. It is essential that all continuity conditions be satisfied along the surface. The usual families of basis functions fail to satisfy these conditions at the ends. The method that was derived maps the modes of a perfectly spherical shell onto the meridian. Because of the change in surface shape, these are uncoupled modes for the shell. Consequently, the modal displacement amplitudes are fully coupled. This approach is equally valid for axisymmetric and asymmetric responses, as was demonstrated by comparing the vibrational modes of a long hemi-capped cylindrical shell with predictions obtained from SARA-2d. The significant feature of the formulation, beyond its robustness, is the suitability of the mapped-spherical-mode basis functions for the scales analysis. This feature stems from the fact that the highest wavenumber contained in each basis function is one greater than the preceding.

In addition to verifying the modal vibration properties of a shell in a vacuum, SARA-2d was also used to validate results for a very slender geometry at a representative mid-range frequency (tip-to-tip aspect ratio of six and $ka = 4$). The results obtained from the two methods were in remarkably close agreement. Comparable computations have not been reported in the open literature. Thus, in addition to providing certainty of the formulation for further work investigating scales, the modeling efforts performed here provide realistic benchmarks by which individuals working in structural acoustics may verify their work.

V. CONCLUSIONS

We have presented here a new approach to examining structural acoustics problems: expansion of relevant *structural* details in terms of a spectral series and chapeau distribution.

The research tool presented allows the examination of the effects of elastic scales through the variations of a inertial or elastic distribution. This technique permits evaluation of the interaction and coupling of the total structural and fluid response. The methods and examples presented here can and will used in future research to determine the impact of these scales by considering other locations of the line spring-mass subsystem as well as multiple subsystems. The effects of feature scales on other system parameters is also of interest. However, a more complete analysis method is needed to continue this research. The ultimate goal of this continuing research is to make generalized statements concerning the critical scales in structural acoustics systems. This information will then allow structural acoustic modeling and subsequent analyses to be performed in a more efficient manner.

VI. REFERENCES

1. J. H. Ginsberg, A. D. Pierce and X. F. Wu, "A Variational Principle for Sound Radiation from Vibrating Bodies," Georgia Institute of Technology, No. GTADRL-86-101, (1986).

2. J. H. Ginsberg, K. A. Cunefare and H. Pham, "A spectral description of inertial effects in fluid-loaded plates," in Proceedings of Winter Annual Meeting, ASME (New Orleans, LA, 1993) Vol. 93-WA/NCA-20, pp. 1-8.

3. J. H. Ginsberg and P. Chu, "Asymmetric vibration of a heavily fluid-loaded circular plate using variational principles," *J. Acoust. Soc. Am.*, **91**(2), pp. 894-906 (1992).

4. J. H. Ginsberg and J. G. McDaniel, "An acoustic variational principle and component mode synthesis applied to the analysis of acoustic radiation form a concentrically stiffened plate," *J. Vib. Acoust., Trans. ASME*, **113**, pp. 401-408 (1991).

5. S. Alper and E. B. Magrab, "Radiation from the forced harmonic vibrations of a clamped circular plate in an acoustic fluid," *J. Acoust. Soc. Am.*, **48**(3, pt. 2), pp. 681-691 (1970).

6. M. C. Junger and D. Feit, "*Sound, Structures, and Their Interaction*," (MIT Press, Cambridge, MA, 1986).

7. R. E. D. Bishop and D. C. Johnson, "*Vibration Analysis Tables*," (Cambridge Univ. Press, 1956).

VII. PAPERS, THESES AND REPORTS

Published Papers

1. J. H. Ginsberg and K. Wu, "Nonaxisymmetric acoustic radiation and scattering from rigid bodies of revolution using the surface variational principle," in Acoustic Radiation and Scattering, *ASME*, **NCA-17**, pp. 93-104 (1994).

2. J. H. Ginsberg, K. A. Cunefare and H. Pham, "Spectral description of inertial effects in fluid-loaded plates," *J. Vib. Acoust., Trans. ASME*, **117**(2), pp. 206-212 (1995).

3. W. S. Shepard, Jr., K. A. Cunefare and J. H. Ginsberg, "Identifying critical elastic scales in structural-acoustic models," *J. Vib. Acoust., Trans. ASME*, (submitted for publication).

Presentations

4. J. H. Ginsberg, K. A. Cunefare and H. Pham, "A spectral description of inertial effects in fluid-loaded plates," in Proceedings of Winter Annual Meeting, ASME (New Orleans, LA, 1993) Vol. 93-WA/NCA-20, pp. 1-8.

5. K. A. Cunefare, J. H. Ginsberg and W. S. Shepard, Jr., "A Spectral Description for the Effects of Multiple Point Masses in Fluid-Loaded Plates," 126th Meeting of the Acoustical Society of America, Denver, CO, October 4-8, 1993.

6. K. Wu and J. H. Ginsberg, "Extension of the Surface Variational Principle to Nonaxisymmetric Response of Submerged Thin Shells of Revolution," 127th Meeting of the Acoustical Society of America, Cambridge, MA, June 6-10, 1994.

7. K. A. Cunefare, W. S. Shepard, Jr. and J. H. Ginsberg, "Spectral investigation of spatial scales associated with substructures on a fluid-loaded plate," *J. Acoust. Soc. Am.*, **95**(5, pt. 2), p. 2846 (1994).

8. K. A. Cunefare, W. S. Shepard, Jr. and J. H. Ginsberg, "Spectral techniques for assessing critical scales in models of fluid loaded structures," in Proceedings of 15th International Congress on Acoustics (Trondheim, Norway, 26-30 June 1995) Vol. 4 of 4, pp. 405-408.

9. W. S. Shepard, Jr., K. A. Cunefare and J. H. Ginsberg, "Identifying critical elastic scales in structural-acoustic models.," in Proceedings of ASME, 15th Biennial Conference on Vibration and Noise (Boston, MA, 17-21 Sept. 1995) Vol. B.

10. K. Wu and J. H. Ginsberg, "Progress in Applying the Surface Variational Principle to Analyze Acoustic Radiation from Slender Elastic Bodies," Proceedings of the Symposium on Acoustics of Submerged Structures and Transduction Systems, ASME 15th Biennial Conference on Mechanical Vibration and Noise, Boston, MA, September 17-19, 1995.

11. K. Wu and J. H. Ginsberg, "Extension of the Surface Variational Principle to Nonaxisymmetric Response of Submerged Thin Shells of Revolution," 127th Meeting of the Acoustical Society of America, Cambridge, MA, June 6-10, 1994.

12. J. H. Ginsberg and K. Wu, "Extension of the Surface Variational Principle to Arbitrary Motion of Bodies of Revolution," 123rd Meeting of the Acoustical Society of America, Salt Lake City, UT, May 11-15, 1992.

Theses

13. Kuangcheng Wu, "Wavenumber-Based Formulation of the Surface Variational Principle for Structural Acoustics," Ph.D. thesis, Georgia Institute of Technology, May 1995.

VIII. PARTICIPANTS

Dr. Kenneth A. Cunefare, Principal Investigator
Dr. Jerry H. Ginsberg, technical advisor
W. Steve Shepard, Jr., graduate student, Ph. D. candidate
Kuangcheng Wu, graduate student, (received Ph.D. 9/95)

ONR FINAL REPORT

CONTENTS